PARTICLE ACCELERATION IN SINGLE OR MULTIPLE SOLAR CURRENT SHEETS: THE FINAL SPECTRA.

C. Gontikakis[1], A. Anastasiadis[2], and C. Efthymiopoulos[1]

[1]*Research Center for Astronomy and Applied Mathematics, Academy of Athens, Soranou Efessiou 4, 11527 Athens, Greece, E-mails:cgontik@academyofathens.gr,cefthim@academyofathens.gr*
[2]*Institute for Space Applications and Remote Sensing, Lofos Koufos, 15236 Palea Penteli, Greece, E-mail: anastasi@space.noa.gr*

ABSTRACT

Numerical simulations are presented of the acceleration of charged particles in a single or multiple Harris-type Reconnecting Current Sheet (RCS). We start with thermal (Maxwellian) initial particle distributions at $\simeq 2 \times 10^6$ K. The main goal is to understand how acceleration in a reconnection site affects the final form of the energy and pitch angle distributions, as well as the X-Ray spectra produced on the assumption of a thick target model. These quantities are explored in a parametric space including a) the particle species, b) the relative strengths of the magnetic and electric field components, and c) the number of successive scattering events in a reconnection site including multiple RCSs with random orientation and field parameters. The numerical results are compared to analytical estimates obtained from our previous studies (i.e. [4], [5]).

Key words: Sun; Reconnecting current sheets; particles' acceleration; Solar flares; X-rays.

1. INTRODUCTION

A number of authors have considered particles' orbits in various reconnecting current sheet (RCS) topologies (see [4], [5] and reference there in). In our above cited works we used rigorous analytical methods from the theory of dynamical systems in order to study in detail the orbits of particles in RCSs.

In the present work we consider ensembles of particles that are accelerated in a site of reconnection. The initial distribution is taken to be thermal, corresponding to a coronal temperature. We argue below that, while the energy spectra may be narrow, power laws arise naturally even in a scattering event with a Harris-type RCS when one looks at the X-Ray spectra obtained from the final particle distribution via a thick target modelling.

Furthermore, the energy distribution also broadens when one considers multiple encounters of the particle distribution with RCSs randomly oriented in, e.g., a flaring site. Such an investigation is based on the scenario of the existence of multiple dissipation sites in flares (see [7], [1]).

2. COMPUTATION SET UP

Our model for a single current sheet is the same as in [4], [5] and [6], namely the steady-state electric and magnetic fields are given by:

$$\begin{aligned} \mathbf{E} &= (0, 0, E) \\ \mathbf{B} &= (-y/a, \xi_\perp, \xi_\parallel) B_0 \quad \text{for } |y| \le a \quad (1) \\ \mathbf{B} &= (-sgn(y), \xi_\perp, \xi_\parallel) B_0 \quad \text{for } |y| > a \end{aligned}$$

The magnetic field has two components parallel and perpendicular to the current sheet plane ($\xi_\parallel$, $\xi_\perp$). The edges of the current sheet are at $y = \pm a$ and we do not integrate the particles' orbits beyond these edges. Taking advantage of the translational symmetry of the problem in the z-direction, the equations of motion can be cast in the form of Hamilton's equations under a two degrees of freedom Hamiltonian:

$$H = \frac{1}{2}p_y^2 + \frac{1}{2}(c_4 + \frac{1}{2}y^2)^2 + \frac{1}{2}(I_2 - \xi_\perp z + \xi_\parallel y)^2 - \epsilon z \quad (2)$$

with canonical pairs $(y, p_y = \dot{y})$ and $(z, c_4 = \dot{z} - \frac{1}{2}y^2)$. The quantity I_2 is a second integral of motion given by:

$$I_2 = \dot{x} - \xi_\parallel y + \xi_\perp z \quad (3)$$

which yields the time evolution of the $(x, \dot{x})$ variables missing from Eq.(2). Eq. 2 is given in units in which the main magnetic component is set equal to $B_0 = 1$, the half-thickness $a = 1$, and the electric field is scaled as $\epsilon = E\,m/(aB_0^2 e)$, where m and e are the particle's mass and charge respectively. An electric field E of 100 V/m corresponds to $\epsilon = 10^{-5}$ for electrons and $\epsilon = 0.0184$ for protons due to dependence on the particle's mass. The inverse gyrofrequency $\omega_B^{-1} = m/qB_0$ is taken as the unit of time, equal to 5.7×10^{-10} sec for electrons and 10^{-6} sec for protons.

The particles motion in the RCS is studied by integrating numerically the equations of motion in the above 2D-Hamiltonian. In the present study, the initial conditions of
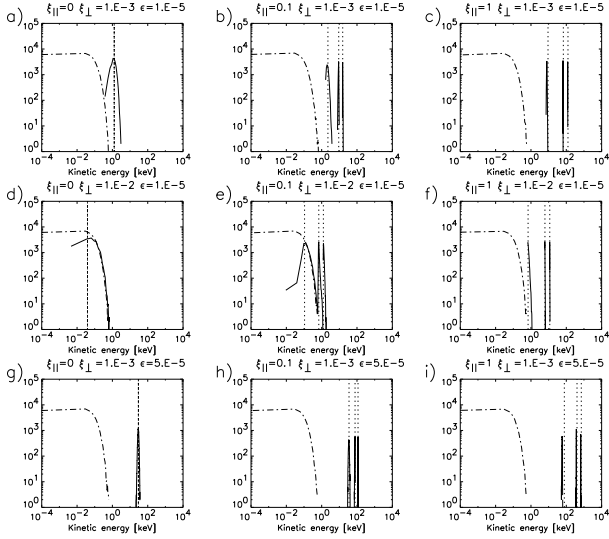
Figure 1. Electron kinetic energy distributions. In each panel, three sets of 10 000 particles are injected from a different initial position $y = 0.9, 0,$ or -0.9. Thus each plotted distribution represent 30000 electrons. For the panels in the first column (panels a, d, g) $\xi_\parallel = 0$. For panels in second column (b, e, h) $\xi_\parallel = 0.1$ and for panels in the third column (c, f, i) $\xi_\parallel = 1$. For panels in the first row (a,b,c) $\xi_\perp = 10^{-3}$ and $\epsilon = 10^{-5}$. For panels in the second row $\xi_\perp = 10^{-2}$ and $\epsilon = 10^{-5}$. For panels in the third row $\xi_\perp = 10^{-3}$ and $\epsilon = 5 \times 10^{-5}$. Vertical dotted lines correspond to an analytical estimation of the kinetic energy gain (see [4]). The point dashed lines correspond to the initial kinetic energy distribution.
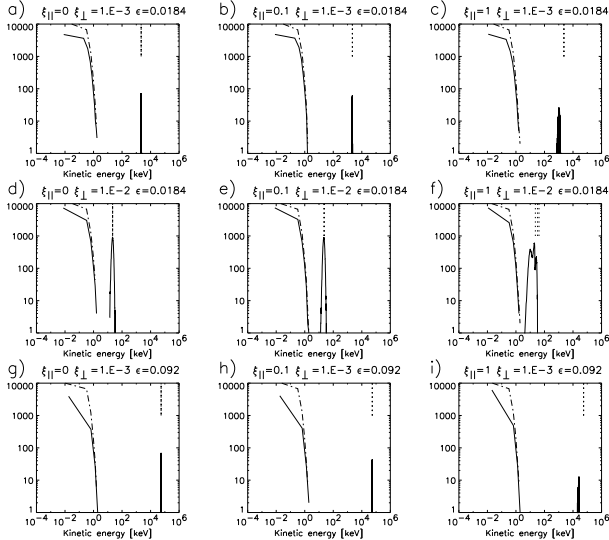

Figure 2. Proton kinetic energy distributions. Same as in Fig. 1 but for $\epsilon = 0.0184$ in the first and second rows and $\epsilon = 0.092$ in the third row. Notice that a fraction of protons is not accelerated.
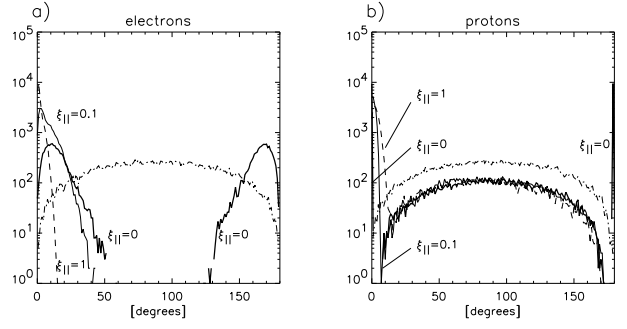

Figure 3. Final pitch angle distributions for the same numerical simulations as in Fig. 1 & 2, panels a, b, c. Panel a shows the electrons pitch angle distributions and panel b the proton pitch angle distributions. For electrons, larger values of $\xi_\parallel$, corresponds to steeper pitch angle distributions. For protons, larger values of $\xi_\parallel$, corresponds to broader pitch angle distributions. The point dashed lines corresponds to the initial pitch angle distributions.

individual particles are selected from a Maxwellian distribution at coronal temperature ($T \simeq 2 \times 10^6$ K).

Orbital integration is performed up to 10^5 time steps in a time interval corresponding to 50 μsec for electrons and to 0.1 seconds for protons. Integration of an orbit ceases when a particle reaches the edges $y = \pm 1$, where we consider the particle as escaping the current sheet. We calculate kinetic energy distributions, pitch angle distributions, times of escape and also store the side of escape ($y = 1$ or $y = -1$). We consider several values of the magnetic and electric field dimensionless parameters within the ranges: $\xi_\parallel = 0., 0.1, 1, \xi_\perp = 10^{-3}, 10^{-2}, \epsilon = 10^{-5}, 5 \times 10^{-5}$. $\xi_\parallel = 1$ corresponds to a magnetic field of 100 Gauss.

3. SINGLE RCS ENCOUNTER

In most cases, the kinetic energy gain is restricted in a relatively small energy range (see Fig. 1). In some field configurations particles do not gain kinetic energy at all (see Fig 1d for electrons). Especially, a fraction of protons are not accelerated (see Fig 2). The final pitch angle distribution of accelerated particles is, in general, narrower than initially depending on the field parameters (see Fig 3).

4. MULTIPLE RCS ENCOUNTERS

We consider consecutive encounters of a distribution of particles with RCSs randomly oriented inside a flaring active region. The initial condition is an isotropic thermal distribution of particles entering the first current sheet from the top or bottom edge. The values of the field components of the sheet are selected randomly, with a uniform distribution in the intervals $\xi_\parallel = 0 - 1, \xi_\perp = 10^{-3} - 10^{-2}$, and $\epsilon = 5 \times 10^{-6} - 3 \times 10^{-5}$ for electrons or $\epsilon = 0.00368 - 0.0552$ for protons. In addition we
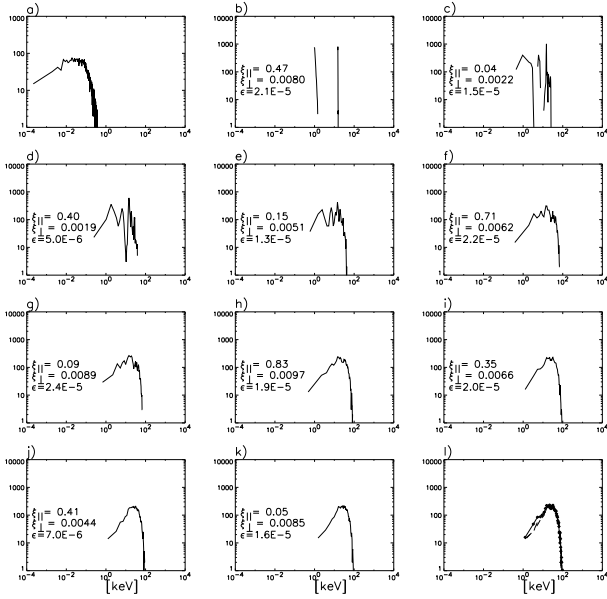
Figure 4. A Maxwellian distribution of electrons (panel (a)) interacts successively with 10 current sheets. In panels (b) to (k) the kinetic energy distributions is shown after the particles have left the current sheet. In each panel, the parameters of the current sheet $\xi_\parallel$, $\xi_\perp$ and ϵ are presented. In panel (l) the kinetic energy distributions of panels (i), (j) and (k) are presented together.

randomize the directions of motion, i.e. the entry pitch angles into a second sheet, while we keep the modulus of the velocity of each particle unchanged, i.e., equal to the exit value from the first sheet (this cannot be changed by magnetic fields).

The main result of Fig. 4 and 5 is that, after a number of encounter events (of the order ~ 10), the kinetic energy distribution appears to *converge to a final form*. Thus, if we superpose the distributions of panels (i), (j), (k) (panel (l)) we obtain a practically unaltered distribution. This limiting distribution marks also the maximum gain of kinetic energy that can be achieved through the multiple scattering process. The final energies reach a limit of $\simeq 100$ keV for electrons and 10^3 keV for protons.

We may understand theoretically the tendency of the energy distributions to 'freeze' by using analytical results from our previous work ([4] [5]). For given initial kinetic energy E_0 and field parameters, the maximum kinetic energy gain is given by:

$$E_{max} = \frac{\epsilon}{\xi_\perp^2}\Big(\xi_\perp I_2 + \xi_\parallel \xi_\perp y_{out} + \epsilon + \qquad (4)$$
$$\sqrt{2\xi_\perp I_2 \epsilon + 2\xi_\parallel \xi_\perp y_{out}\epsilon + \epsilon^2 + 2\xi_\perp^2 E_0}\Big)$$

The value of E_{max} can be computed easily from the initial conditions of the orbit $\dot{x}_0, y_0, z_0$ for $y_{out} = 1$, by setting $z_0 = 0$ (without loss of generality) and $I_2 = \dot{x}_0 - \xi_\parallel y_0$. If we divide the cubic parameter space $(\xi_\parallel, \xi_\perp, \epsilon)$ in a lattice of $10 \times 10 \times 10 = 1000$ grid points, we can
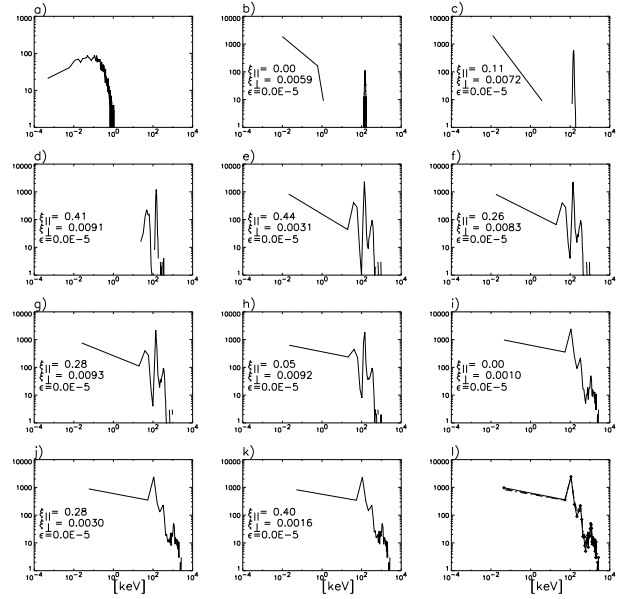

Figure 5. Same as Fig. 4 but for protons.

calculate the number of points $N(E_0, F)$ (out of 1000) for which the maximum final energy was larger from the initial energy E_0 by a factor F. Now, as analyzed in our previous papers, as E_0 increases, the chance that an electron is significantly accelerated decreases, thus, for fixed factor F, we expect N to be a decreasing function of E_0. Precisely, this is shown in Fig. 6, for $F = 2$, (a) for electrons, (b) for protons. In (a) we see that when the initial kinetic energy of an electron reaches a value $\simeq 120$ keV, only 3% of parameter values in the cubic lattice considered can yield current sheets that act as accelerators efficient enough so as to double the kinetic energy of the particles. Thus, when the electron kinetic energy distribution is shifted to values of order 100 keV, a further increase in the energy becomes a rare event that can occur only for some specific combinations of the values of the magnetic and electric fields covering a small sub-volume of the total parameter space. The same is true for protons when E_0 reaches a value $\simeq 4$ MeV (panel b). In both cases, we found that when the particle distributions approach the limiting distributions, they remain practically invariant for larger and larger numbers of iterations. Only marginal shifts to the right occasionally take place by 'kicks' which become less and less frequent as the number of iterations increases.

5. X-RAY COMPUTATION

Assuming a model of 'thick target radiation' (see [3], [2] and [8]), it is possible to compute X-ray spectra that correspond to a particular electron kinetic energy distribution. In the thick target approach, the electrons, after escaping from the accelerator region, have impacts with a dense medium (e.g. the chromosphere) where they lose their kinetic energy in very small times via bremsstrahlung radiation (there is practically no modifi-
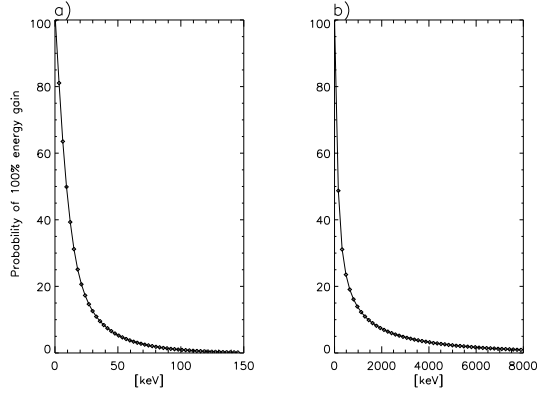
Figure 6. *Probability for an electron (panel a) or a proton (panel b), with a given initial kinetic energy E_0, (shown in the horizontal axis) to leave a current sheet with a final kinetic energy of $2E_0$. Electrons with $E_0 = 100$ keV have 0.9% chances to enter a current sheet which will accelerate them at 200 keV. Moreover, protons with $E_0 = 4000$ keV have 3% chances to a current sheet which will accelerate them at 8000 keV*

cation due to transport). The computation of the X-ray spectrum produced by bremstruhlung radiation starts by considering the number of photons of energy $h\nu$ emitted by an electron of initial energy E_0.

$$\mu(h\nu, E) = \int_{E_0}^{h\nu} \sigma(h\nu, E) n_p v(E) \frac{dE}{dt} dt \qquad (5)$$

where $\sigma(h\nu, E)$ is the cross-section coefficient of the bremshtruhlung emission, n_p the density of the ambient plasma $v(E)$ the electron's velocity and dE/dt the energy loss due to collisions. Then, the photon spectrum emitted by an electron distribution $F(E_0)$ in the range $E_0, E_0 + dE$ is given by the integral:

$$I(h\nu) = \int_{h\nu}^{+\infty} F(E_0) \mu(h\nu, E_0) dE_0 \qquad (6)$$

For each electron kinetic energy distribution we computed a corresponding X-ray spectrum. The computations involve only the part of a kinetic energy distribution above 1.6 keV. In some distributions with maximal kinetic energies reaching $\simeq 3$ keV the X-ray computation becomes irrelevant. Typical computed X-ray spectra are shown in Fig. 7. The maximum photon energy is lower but close to the maximum electron kinetic energy.

The main result is that, contrary to the particle distributions, the spectrum is a smooth curve that decreases monotonically with increasing photon energy, up to a limit corresponding to the highest reached photon energy, at which the spectrum exhibits an abrupt fall. As the X-ray spectrum is computed through the integral of Eq 5), the presence of peaks in the particle kinetic energy distributions is smoothed out. Furthermore, the spectrum corresponding to a multiple event (Fig 7d) shows a decrease that is less abrupt as the photon energy increases. The spectra of Figs 7c,d, yield values of the maximum
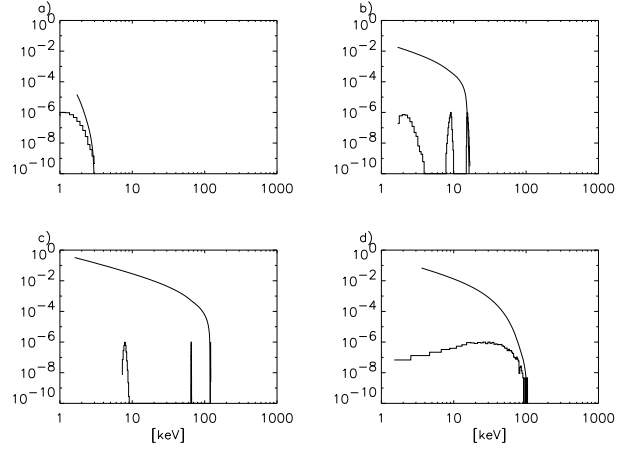

Figure 7. *X-ray spectra compared with the kinetic energy distribution which produce them. In panel (a), $\xi_\parallel = 0$, in panel (b) $\xi_\parallel = 0.1$ and in panel (c) $\xi_\parallel = 1$. In panels (a) to (c) $\xi_\perp = 10^{-3}$ and $\epsilon = 10^{-5}$. In panel (d), the kinetic energy distribution is produced by a multi sheets experiment and is the same as in Fig. 4(k). The kinetic energy distributions are shown as an histogram and are put into scale.*

photon energy at $\simeq 100$ keV. This compares well with non-thermal X-ray observations.

ACKNOWLEDGEMENTS

REFERENCES

[1] Anastasiadis A., J. Atm. Sollar - Terr. Phys., 64(5-6), 481, 2002.

[2] Anastasiadis A., Gontikakis C., Vlimer N. and Vlahos L., Astron. Astrophys. , 422, 323., 2004.

[3] Brown J.C., Solar Phys., 18, 489, 1971.

[4] Efthymiopoulos C., Gontikakis C. and Anastasiadis A., Astron. Astrophys., 443, 663, 2005.

[5] Gontikakis C., Efthymiopoulos C. and Anastasiadis A., Mon. Not. R. Astron. Soc., 368(1), 293., 2006.

[6] Litvinenko Y. and Somov B., Solar Phys., 146, 127, 1993.

[7] Parker E., Astrophys. J., 330, 474., 1988.

[8] Vilmer N., Solar Phys. 111, 207, 1987.